

# SECONDARY INSTABILITY OF EKMAN LAYER ROLLS

T. Dubos, C. Barthlott, C. Fesquet and P. Drobinski  
IPSL/LMD, École Polytechnique, France

## Abstract

We<sup>1</sup> study the non-linear stages of the instability of the neutrally-stratified Ekman flow. We find that two-dimensional equilibrated rolls exist, and are reached very closely, although not exactly, after a small random initial perturbation to the Ekman flow has evolved and reached nonlinear saturation. We perform in turn a linear stability analysis of these equilibrated rolls and find that they are subject to an instability of the hyperbolic type. In both studies, we investigate the influence of the latitude and of the direction of the geostrophic wind on these stability properties.

## 1 INTRODUCTION

The Ekman spiral flow is an exact solution of the Navier-Stokes equations in the presence of rotation and a rigid boundary. It is useful as a prototype flow for idealized dynamical studies of the planetary boundary layer (PBL). In such studies, the Reynolds number is understood as a turbulent Reynolds number. Values about 500 are considered typical of the PBL [Foster, 1997]. Lilly established that the neutrally-stratified Ekman flow is subject to an inflexion point instability [Lilly, 1966].

The rolls often observed in the neutral planetary boundary layer are usually interpreted as the outcome of this instability. However important characteristics of its non-linear development remain unclear. Indeed, due to nonlinear interactions with itself and the basic flow after the initial stage where the linear approximation is valid, a linearly unstable perturbation may either saturate or directly produce chaos. The convective instability for instance is known to saturate into convective rolls but contradictory conclusions concerning the Ekman flow can be found in the literature. Coleman runs direct numerical simulations at  $Re=400$  and finds no equilibrated rolls [Coleman et al., 1990]. Foster performs high-order amplitude expansions at  $Re=500$  and finds that they admit a steady state. The following questions are addressed in this work :

1. Does the instability saturate, and how ?

<sup>1</sup>Corresponding author address : Thomas Dubos, LMD École Polytechnique, 91128 Palaiseau, France ; E-mail : dubos@lmd.polytechnique.fr

2. How stable or unstable are the equilibrated rolls with respect to three-dimensional perturbations ?

The magnitude of the horizontal component of the Coriolis vector and its direction with respect to the geostrophic wind are known to influence the domain of primary instability [Leibovich and Lele, 1985]. We investigate their influence on the nonlinear saturation and on the secondary instability as well.

## 2 SATURATION OF THE PRIMARY INSTABILITY

### 2.1 Position of the problem

At latitude  $\lambda$ , the vertical component of the Coriolis vector is  $f = 2\Omega_0 \sin \lambda$ . We scale velocities by the geostrophic wind  $G$  and lengths by the laminar boundary-layer depth  $\delta = \sqrt{2K/f}$  where  $K$  is a constant turbulent viscosity. The fluid obeys the incompressible rotating Navier-Stokes equations written in adimensional form as :

$$\text{div } \mathbf{U} = 0$$

$$\frac{\partial \mathbf{U}}{\partial t} + \nabla \left( P + \frac{\mathbf{U} \cdot \mathbf{U}}{2} \right) + \left( \omega + \frac{2}{Re} (\mathbf{e}_z + \cotg \lambda \mathbf{e}_N) \right) \times \mathbf{U} = \frac{1}{Re} \Delta \mathbf{U}$$

where  $Re = G\delta/K$  is the Reynolds number,  $P$  is the pressure,  $\mathbf{U}$  is the velocity,  $\omega$  is the fluid vorticity,  $\mathbf{e}_z$  is the upward vertical unit vector and  $\mathbf{e}_N$  is the unit vector pointing to the North. Equation (??) admits the well-known Ekman stationary solution :

$$\mathbf{U}_0(z) = (1 - e^{-z} \cos z)(\cos \theta \mathbf{e}_E + \sin \theta \mathbf{e}_N) + e^{-z} \sin z (\cos \theta \mathbf{e}_N - \sin \theta \mathbf{e}_E)$$

where the angle  $\theta$  between the East and the geostrophic wind is arbitrary. Hence the global parameters of the problem are the Reynolds number  $Re$ , the latitude  $\lambda$  and the angle  $\theta$ .

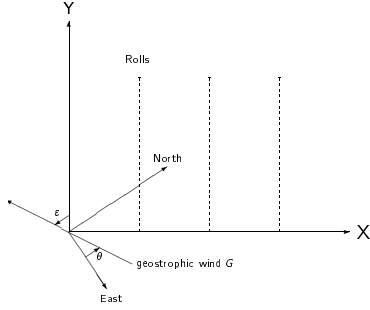


Figure 1: Top view of the horizontal axis system. There is an angle  $\theta$  between the East and the geostrophic wind and an angle  $\epsilon$  between the geostrophic wind and the  $y$  axis (roll axis).

Solving the linear stability problem consists in looking for eigenmodes of the rotating Navier-Stokes dynamics linearized around the basic flow  $\mathbf{U}_0(z)$ . Due to horizontal homogeneity, such eigenmodes vary horizontally like  $\exp(i\mathbf{k}_1 \cdot \mathbf{x})$  for some horizontal wave vector  $\mathbf{k}_1$ . For each  $\mathbf{k}_1$  only the vertical structure of the eigenmode is to be obtained. For given  $\mathbf{k}_1, Re, \lambda, \theta$ , a few discrete eigenmodes, growing like  $e^{\sigma t}$ , are usually found. We note  $\sigma_1(\mathbf{k}_1; Re, \lambda, \theta)$  the largest one. Next, for given  $\mathbf{k}_1, Re, \lambda, \theta$ , the growth rate  $\sigma_1$  reaches a maximum  $\sigma_1(Re, \lambda, \theta)$  at a certain  $\mathbf{k}_1(Re, \lambda, \theta)$ . This selects the preferred horizontal length scale  $l = 2\pi/k_1$  that emerges when the basic flow is perturbed. At latitude  $\lambda = 90^\circ$ , unstable modes appear when the Reynolds number reaches the critical value  $Re_c \simeq 54$  [Lilly, 1966]. The critical Reynolds number is lower at other latitudes [Leibovich and Lele, 1985]. In the sequel, we consider the nonlinear saturation of this most unstable eigenmode.

## 2.2 Stationary rolls : existence and spatial structure

We run a direct numerical simulation at  $Re=500$ . At this Reynolds number, the growth rate of the primary instability is  $\sigma_1 = 0.024$ . This maximum is reached for  $k_1 = \|\mathbf{k}_1\| \simeq 0.5$  and for an angle between the roll axis and the geostrophic wind of  $\epsilon \simeq 17^\circ$  (see figure 1). In the simulation, the velocity field depends only on the vertical coordinate  $z$  and the horizontal coordinate  $x = \mathbf{x} \cdot \mathbf{k}_1/k_1$ . The  $x$  direction is periodic with wavelength  $2\pi/k_1 \simeq 12$  so that exactly one period of the most unstable mode fits in

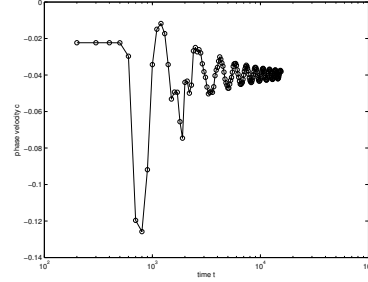


Figure 2: Time evolution of the phase velocity  $c$  during the nonlinear saturation of the unstable mode.

this domain. The initial condition is random with amplitude  $10^{-5}$ .

At each time we compute the phase velocity  $c(t)$  of the flow by minimizing the r.m.s of  $\partial\mathbf{U}/\partial t + c\partial\mathbf{U}/\partial x$ . We display the evolution of  $c(t)$  on figure 2. The linear stage can be identified as the interval where  $c$  is equal to the eigenmode-based prediction  $c \simeq -0.022$ . Later, nonlinear interactions become dominant and drive the flow to a travelling quasi-equilibrium. A drastic change in the phase velocity  $c(t)$  occurs during a transient phase of duration on the order of a few  $\tau = 1/\sigma \simeq 40$ . The phase velocity then relaxes towards a value  $c \simeq -0.04$ , still presenting slow oscillations with a period of several tens of  $\tau$ . These oscillations decay but even more slowly.

Next we search for an exactly equilibrated flow, i.e a flow  $\mathbf{U}_1(x, z; Re, \lambda, \theta)$  and a phase velocity  $c$  such that  $\partial\mathbf{U}_1/\partial t + c\partial\mathbf{U}_1/\partial x = 0$  where  $\partial\mathbf{U}_1/\partial t$  is defined by the Navier-Stokes equation (??). We use Newton's iteration and take as a first guess the quasi-stationary flow reached at the end of the simulation. Very small corrections are enough to reduce  $\partial\mathbf{U}/\partial t + c\partial\mathbf{U}/\partial x$  to machine precision. It is customary in linear stability studies to display the perturbation fields but once nonlinear saturation has been reached it is more instructive to display the total flow, as we do in figure 3. The roll axis is perpendicular to the figure. Isolines of axial (along-roll) vorticity emphasize the vortical structure of the saturated flow. There is one vortex per spatial period so that the periodic flow presents a pattern of co-rotating vortices. The vortex is fairly broad, with a small core located around  $x \simeq 3$ . Under this broad vortex, a secondary, intensified boundary layer is formed. In the absence of the Coriolis force, the axial velocity would be simply advected by the flow in the  $(x, z)$  plane and diffused by viscosity. This explains the ejection of low axial

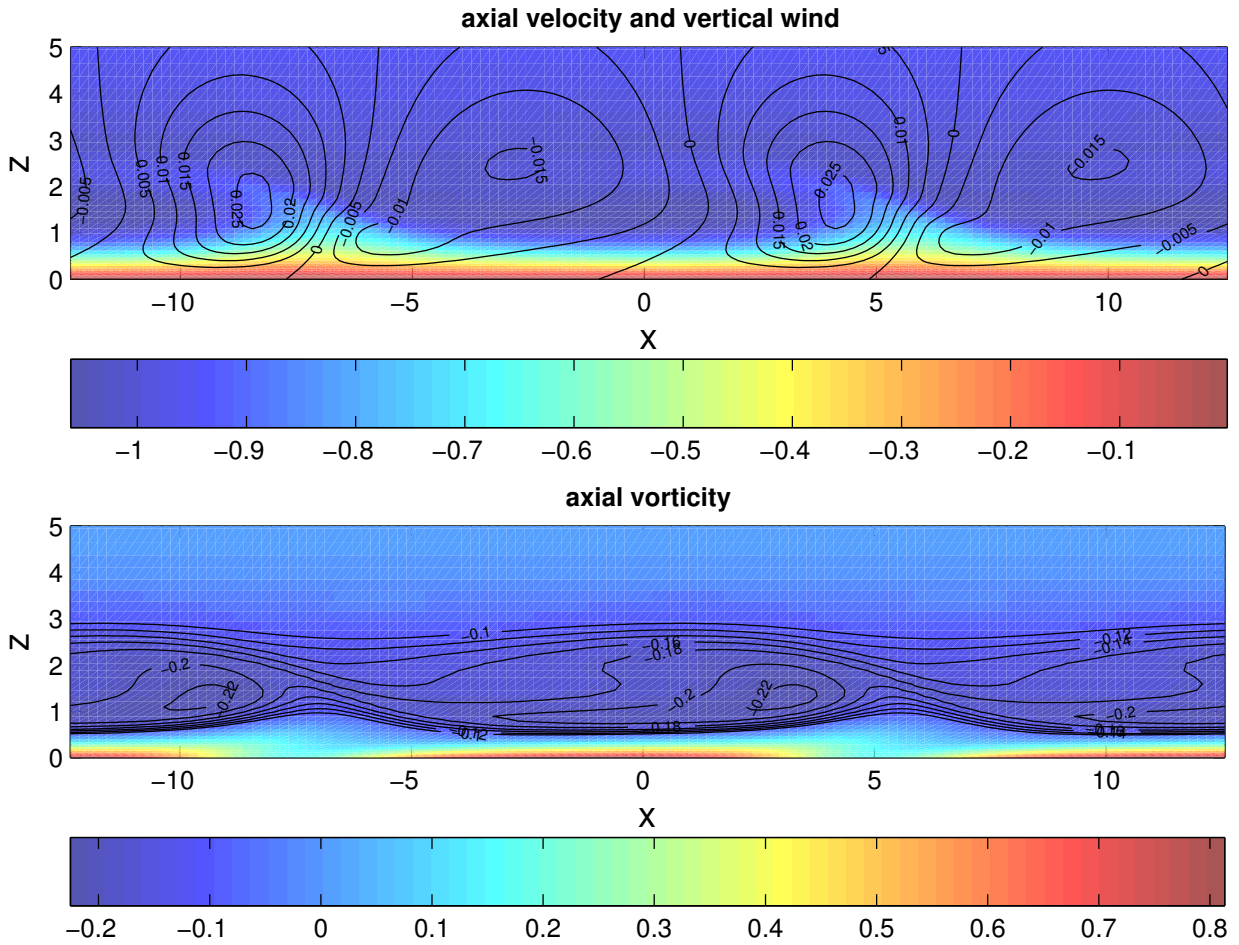


Figure 3: Spatial structure of the saturated rolls for  $Re = 500$  and  $\lambda = 90^\circ$ . The rolls are perpendicular to the  $X$  axis. Two spatial periods  $2\pi/\|\mathbf{k}_1\| \simeq 12$  are presented. Top : axial velocity (color) and vertical velocity (contours). Bottom : axial vorticity (color and contours).

velocity between two consecutive rolls, visible near  $x \simeq 5$ .

### 2.3 Dependence on latitude

The latitude influences the problem through the horizontal component of the Coriolis vector, but is affected by a weight inversely proportional to the Reynolds number. Hence one may expect a vanishing influence as  $Re \rightarrow \infty$ . Indeed the growth rates of the primary instability tend to depend less and less on latitude as the Reynolds number grows [Leibovich and Lele, 1985]. However a sensitivity of the Reynolds stress to latitude was observed by Coleman at  $Re = 400$  [Coleman et al., 1990]. Hence despite its small absolute magnitude the coupling induced by the horizontal part of the Coriolis vector between the different velocity components may have a significant overall effect.

We reproduced the previous steps at latitude  $\lambda = 45^\circ$  for wind blowing from the four cardinal directions. As far as the stationary rolls are concerned, very little dependence was observed. The vertical velocity field, which is zero in the Ekman spiral flow, is a good indication of the vortex intensity. We found that the difference between  $\lambda = 45^\circ$  and  $\lambda = 90^\circ$  is less than 2% in a root-mean-square sense.

## 3 SECONDARY INSTABILITY OF SATURATED ROLLS

In the previous section we have found saturated rolls, which are stationary solutions of the rotating Navier-Stokes equations (??) in a Galilean referential travelling with a nonlinear phase velocity  $c$ . Such columnar vortices are subject to different families of secondary instability. The Kelvin-Helmholtz rolls that result from the saturation of a free-shear instability are known to suffer in neutral or stable stratification from elliptic and hyperbolic instabilities [Peltier and Caulfield, 2003]. Unlike Kelvin-Helmholtz rolls, saturated Ekman rolls have axial velocity, like swirling jets. This produces shear along the roll axis and may result in another type of instability. The presence of a rigid boundary could affect the stability properties as well.

### 3.1 Growth rates and latitude

We consider the growth or decay of infinitesimal, three-dimensional perturbations to the secondary flow  $\mathbf{U}_1$ . Due

to the invariance of the problem along the roll axis ( $y$  direction), and periodicity in the  $x$  direction the normal modes of instability are of the form  $\hat{\mathbf{U}}(x, z) \exp i\mathbf{k}_2 \cdot \mathbf{x}$ . The secondary wavenumber  $\mathbf{k}_2$  has a component  $\gamma$  along the roll axis ( $y$  direction) and a component  $\beta$  in the  $x$  direction. For given  $\gamma$  and  $\beta$ , the growth rate  $\sigma_2(\gamma, \beta; Re, \lambda, \theta)$  is the eigenvalue with largest real part of the operator resulting from the linearization of the rotating Navier-Stokes dynamics around the basic state  $\mathbf{U}_1(x, z; Re, \lambda, \theta)$ .

We first consider the latitude  $\lambda = 90^\circ$ . One can show that  $\sigma_2(\gamma, \beta; Re, \lambda, \theta) = \sigma_2(\gamma, \beta + k_1; Re, \lambda, \theta)$  and this is what we obtain (not shown). Furthermore the dependence of  $\sigma_2$  on  $\beta$  is extremely weak with relative fluctuations on the order of 1%. We display in figure 4 the growth rate  $\sigma_2$  as a function of the axial wave vector  $\gamma$  which is the important parameter. Wave numbers  $1.1 \leq \gamma \leq 2.8$  are unstable with a maximum growth rate  $\sigma_2 \simeq .021$  reached for  $\gamma \simeq 1.9$ . Hence the time scale for the secondary instability is comparable to that of the primary instability while the selected length scale is about four times shorter since  $k_1 \simeq 0.5$ .

We next consider the latitude  $\lambda = 45^\circ$  and wind blowing from the four cardinal directions. All stability curves are nearly identical, with the notable exception of wind blowing to the East. For this direction, the unstable domain is slightly reduced, the most unstable wave vector is roughly identical and the maximum growth rate is reduced by about one third. Since the corresponding basic flows are almost identical, this is a non trivial effect of the horizontal component of the Coriolis vector. Further insight may be gained by inspecting the energetics of these modes, e.g. how they extract their energy from the basic flow.

### 3.2 Structure of the unstable modes

We display in figure 5 the amplitude  $\|\hat{\mathbf{U}}(x, z)\|$  of the most unstable mode at  $Re = 500$  and latitude  $\lambda = 90^\circ$ . The mode is very localized, along the vorticity filament that connects one roll to the next. This filament results from the strong stretching by the flow in the  $(x, z)$  plane around a hyperbolic stagnation point. This is therefore strongly suggestive of an hyperbolic instability [Godefert et al., 2001]. Notice however that this region also experiences a strong axial shear, e.g. the axial velocity has strong gradients in this region. Hence another possibility would be an axial shear instability.

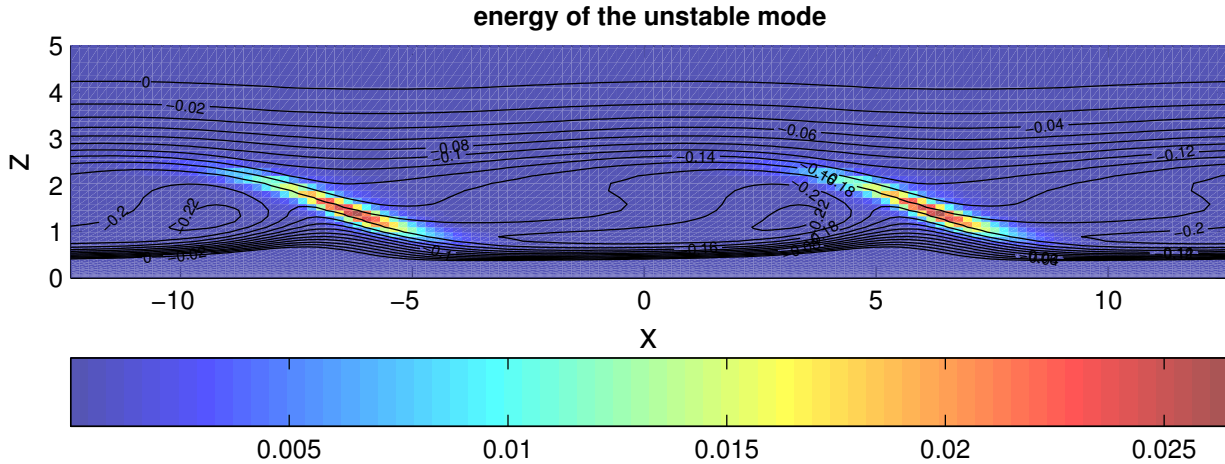


Figure 5: Amplitude  $\|\hat{\mathbf{U}}(x, z)\|$  of the unstable mode. Black : isocontours of downstream vorticity.

## 4 Discussion

We find that equilibrated rolls exist, and are reached very closely, although not exactly, after a small random initial perturbation to the Ekman flow has evolved. Interestingly, while the observations mention contra-rotating rolls, these equilibrated rolls are co-rotating, as one would expect from the saturation of the instability of a parallel shear flow. The structure of these rolls depends very little on the horizontal component of the Coriolis vector. Although we do not present this here, these stationary solutions can be used to obtain quantitative estimates of roll-induced Reynolds stresses, as a function of the (turbulent) Reynolds number.

We find that these rolls are unstable with respect to three-dimensional perturbations, probably through a mechanism of hyperbolic instability. More detailed investigations are needed to elucidate the precise mechanism of instability, and to understand how the small horizontal component of the Coriolis vector can have a significant stabilizing effect for certain wind directions.

Finally the nonlinear evolution of the three-dimensional instability. It may saturate or lead directly to the disruption of the roll vortices, as is the case in weakly-stratified, free-shear instability [Peltier and Caulfield, 2003]. This should be investigated in order to discuss further the relevance of the inflexion-point instability for the emergence of ABL rolls.

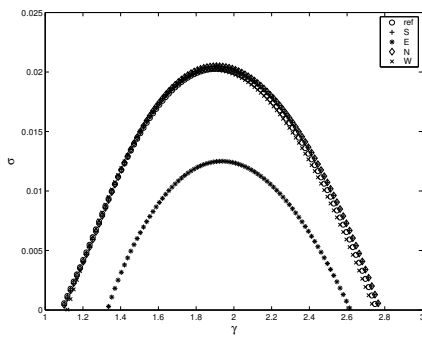


Figure 4: Growth rate of the secondary instability as a function of the axial wavenumber  $\gamma$  for  $Re = 500$ . Solid : latitude  $\lambda = 90^\circ$ . Others : latitude  $\lambda = 45^\circ$ , geostrophic wind blowing to the South, East, North, West.

## Appendix : Numerical methods

The velocity field being non-divergent is completely described by the vertical velocity and the vertical vorticity. These two scalar dynamical fields are decomposed on a set of basis functions that satisfy the appropriate boundary conditions. As a result, computing the pressure is never required [Spalart et al., 1989, Coleman et al., 1990]. This spatial discretization is spectrally accurate. The  $z$  direction goes from  $z = 0$  to  $z = \infty$ , with high resolution near  $z = 0$  and progressively poorer resolution as  $z$  increases. We use 64 quadrature points in each direction. The highest quadrature point is at  $z = 32.7$  and 50% of the quadrature points are below  $z = 3$ .

In order to study the transient phase of saturations, we perform temporal integrations, using a third-order Adams-Bashforth scheme with implicit treatment of viscosity. When searching for exactly equilibrated rolls, each Newton iteration involves the resolution of a linear system with several thousands of unknowns. Addressing the linear stability of these saturated rolls is an eigenproblem of comparably large size. Direct methods are inappropriate for such large problems and we use matrix-free, iterative methods to solve them. For the linear system we use the Generalized Minimal Residual method (GMRES) preconditioned by the Poisson operator. For the eigenproblem we use a variant of the implicitly restarted Arnoldi iteration providing the eigenvalue with largest real part [Lehoucq et al., 1997].

## References

- [Coleman et al., 1990] Coleman, G., Ferziger, J., and Spalart, P. (1990). A numerical study of the turbulent Ekman layer. *J. Fluid Mech.*, 213:313–348.
- [Foster, 1997] Foster, R. (1997). Structure and energetics of optimal Ekman layer perturbations. *J. Fluid Mech.*, 333:97–123.
- [Godefert et al., 2001] Godefert, F., Cambon, C., and Leblanc, S. (2001). Zonal approach to centrifugal, elliptic and hyperbolic instabilities in Stuart vortices with external rotation. *J. Fluid Mech.*, 449:1–37.
- [Lehoucq et al., 1997] Lehoucq, R. B., Sorensen, D. C., and Yang, C. (1997). *ARPACK Users' Guide: Solution of Large Scale Eigenvalue Problems with Implicitly Restarted Arnoldi Methods*. <http://www.caam.rice.edu/software/ARPACK/>.
- [Leibovich and Lele, 1985] Leibovich, S. and Lele, S. (1985). The influence of the horizontal component of earth's angular velocity on the instability of the Ekman layer. *J. Fluid Mech.*, 150:41–87.
- [Lilly, 1966] Lilly, D. (1966). On the instability of Ekman boundary flow. *J. Atmos. Sci.*, 23(481-494).
- [Peltier and Caulfield, 2003] Peltier, W. and Caulfield, C. (2003). Mixing efficiency in stratified shear flows. *Annu. Rev. Fluid Mech.*, 35:135–167.
- [Spalart et al., 1989] Spalart, P., Moser, R., and Rogers, M. (1989). Spectral methods for the Navier-Stokes equations with one finite and two periodic directions. *J. Comput. Phys.*, 96:297–324.